

UNDERWATER EXPLOSIONS

C. W. Hirt
Flow Science, Inc.
November 1989

INTRODUCTION

Underwater explosions and their effects are important for many activities including ocean engineering risk analysis, naval ship survivability studies, the breakup of river ice, and underwater seismic investigations. The hydrodynamic effects induced by underwater explosions vary widely depending on the charge size, its depth below the free surface, the local bathymetry, and the presence of nearby structures.

In this note we present the results of a single FLOW-3D calculation that models an explosion occurring below a cylindrical structure. For simplicity, a two-dimensional, axisymmetric problem has been chosen to demonstrate how FLOW-3D may be used to investigate the effects of underwater explosions. Because this problem includes a nearby rigid structure and a free surface, it serves as a good generic test problem.

THE PROBLEMPhysical Description

Figure 1 shows a schematic of the problem. A rigid cylindrical body having a diameter of 40 ft extends 15 ft below the surface of the water. Located on the cylindrical axis, 10 ft below the base of the cylinder, is an explosion gas bubble. The bubble has an initial radius of 1.91 ft and is filled with gas at a pressure of 11,800 psi. It is assumed that the explosion products can be approximated by a polytropic gas with a ratio of specific heats equal to 1.25.

Above the free surface of the water there is a constant air pressure of 14.7 psi. At time zero the water is assumed to be at rest. This means that any effects of shock waves or other disturbances arising from the original explosion are neglected in comparison with the subsequent effects generated by the high pressure gas bubble. In fact, the water will be treated as a strictly incompressible fluid. FLOW-3D could be used to model the early time compressibility effects, but this is beyond the scope of the present investigation.

Numerical Description

For computations it is necessary to limit the region to be modeled. Ideally we would like to place the computational boundaries as far away from the explosion region as possible so that they will not influence the computed results. Making the region too large, however, can lead to excessive computational costs. We have chosen a compromise and tried to minimize the influence of computational boundaries with the use of special FLOW-3D boundary conditions.

At the outer radial boundary a hydrostatic pressure and fixed fluid height condition have been used. Flow may pass in or out through this boundary, but the pressure distribution and fluid free surface at this boundary never change. Additionally, we have used the code option that treats the boundary pressure as a stagnation pressure; i.e., any flow entering the computing region through this boundary must be accelerated from rest at the boundary pressure.

At the bottom of the computational region there is a rigid, free-slip boundary. The left edge of the computing region is an axis of cylindrical symmetry, while at the top boundary a rigid lid may be used since no flow reaches this boundary. In the plots presented later we show a complete cross section with the axis of symmetry located in the middle of the plots, however, it should be remembered that only the right half of the flow has actually been computed.

The water density is 1.94 slugs per cubic ft and gravity is taken to be 32.2 ft/s/s. In order to have pressures in units of psi we have reduced the water density in the calculation by a factor of 144. This mixing of units must be kept in mind when evaluating the computed forces on the cylinder. In particular, it is necessary to multiply the computed force values by 144 to get pounds force and by another factor of 13.66 to get the force on the complete cylinder (since we are only modeling 1/13.66 azimuthal segment of the cylinder). Thus, the computed axial force must be multiplied by 1967 to obtain the total axial force on the cylinder in pounds.

The computational mesh used for the calculations consists of 27 radial and 55 axial mesh cells, or a total of 1485 interior cells. The smallest cell sizes in the radial and axial directions are 0.5 ft and are located at the center of the gas bubble. This is necessary because of the small size of the initial bubble. The grid is stretched away from the bubble in order to keep the total number of cells to a reasonable level.

A complete FLOW-3D input file for the problem is given in Fig. 2. This file defines the grid, geometry, initial fluid configuration, pressures, and all other parameters needed for the calculation. The file also specifies where selected output is desired, in this case the flow histories at the center of the initial bubble and at the bottom center of the cylinder. Because the flow evolves through several phases we have used a variable edit frequency; the early

expansion and late collapse phases of the gas bubble are relatively fast and require a short edit interval compared to the slower intermediate phase when the bubble reaches its maximum expansion. These edit intervals are located at the end of the XPUT input section in Fig. 2.

A new second order option (IORDER=3 in the input) was used for the computation. This increases the calculational CPU time a little bit, but insures better accuracy. The higher order option was used because it was thought that a narrow re-entrant jet might form when the bubble collapsed. After reviewing the computational results it was concluded that the faster, first order approximation would probably have worked about as well.

COMPUTATIONAL RESULTS

Discussion of the computed results can be naturally divided into the bubble expansion process followed by a discussion of the phenomena associated with the subsequent bubble collapse. Theoretically the bubble should undergo multiple oscillations, but in this calculation the bubble is not resolved well enough to allow for this possibility. More discussion about this aspect of the calculation will be given later.

Bubble Expansion

A sequence of plot frames showing the early expansion of the gas bubble is given in Figs. 3-4. Figure 3 contains plots of the fluid configuration and velocity field, while Fig. 4 shows pressure contours at selected times during the expansion. The bubble expands more or less spherically until about $t=0.06$ s when it begins to be affected by the rigid cylinder. The bubble has completely engulfed the base of the cylinder by $t=0.3$ s.

At this time one can also see a vortex flow that develops at the outside corner of the base of the cylinder. It should also be observed that the free surface has been pushed up along the sides of the cylinder because gravity has not yet had time enough to form outward moving waves.

After about 0.01 s the initial bubble pressure is low enough that the pressure contours in Fig. 4 clearly show the hydrostatic pressure at the outer radius of the plots.

The bubble reaches its maximum volume of about 1100 times its initial volume at roughly $t=0.4$ s. This can be seen in the bubble volume history plot, Fig. 5A. (Because the calculation was run in two parts, this history plot only shows the time interval of the first part, which ran to $t=0.7$ s.) The corresponding bubble pressure history is shown in Fig. 5B. Since the pressure decreases with

radius raised to the power of 3.75, we see a very rapid decrease in bubble pressure. The minimum pressure in the bubble occurs at the time of maximum volume and is between 1 and 2 psi.

For comparison, the Rayleigh solution for an adiabatically expanding bubble in an infinite medium with a pressure of 25.54 psi at infinity (i.e., the hydrostatic pressure at the depth of the initial bubble) predicts a maximum volume 1849 times as large as the initial volume. The presence of the rigid cylinder hinders the upward expansion of the bubble. Gravity effects should also reduce its downward expansion somewhat, so the smaller calculated 1100 fold increase in volume seems quite realistic when compared to 1849 for the Rayleigh solution.

Figure 6 gives the axial force on the cylinder for the first portion of the calculation (to $t=0.7$ s). The force decreases rapidly from its initial value to a very low value corresponding to the low gas pressure pushing on the entire base of the cylinder at the time of maximum bubble expansion.

Bubble Collapse

After $t=0.4$ s the bubble begins to recompress. Figure 7 shows the vector plots during this period, while Fig. 8 contains the pressure contours. At $t=0.5$ s the surface of the bubble has become somewhat ragged as the flow tries to decide which way to go. By $t=0.6$ s there is a jet beginning to develop at the bottom of the bubble. The collapse is greatest at this point because this is the location of greatest hydrostatic pressure surrounding the bubble.

The re-entrant jet strikes the center of the cylinder just before $t=0.7$ s. By $t=0.72$ s the surface of the bubble has again become smooth and the bubble is toroidal shaped. As time proceeds the jet spreads out across the base of the cylinder and eventually the bubble is detached from the base shortly after $t=0.78$ s. At this time the numerical resolution is not sufficient to resolve the small cross section of the bubble.

A simple hand calculation shows that if the toroid cross section were circular, its radius would have to be approximately 0.314 ft when the toroidal volume is equal to the initial bubble volume. Since the minimum grid cell width is 0.5 ft, and this size is only at the initial location of the bubble, it is clear that we cannot expect to follow the complete collapse phase of the bubble in this calculation.

Once the bubble resolution is lost, the calculation cannot be accepted as realistic. In particular, the code "forgets" the bubble gas pressure and artificially reduces the pressure in the region of the unresolved bubble in order to close up the residual (subgrid cell) void.

There are some interesting features worth noting in the pressure contour plots shown in Fig. 8. At $t=0.7$ s, for example, a negative pressure exists at the outer edge of the cylinder. This reflects an attempt of the fluid to remain attached to the cylinder as it flows around the corner toward the centerline. The high pressure location at this time is at the point where the re-entrant jet has just struck the cylinder.

Physically, the water should cavitate in the negative pressure region. In FLOW-3D, however, we cannot model cavitation and simultaneously track the evolution of gas bubbles. Fortunately, these negative pressures do not persist so it is unlikely that cavitation plays a significant role in the overall dynamics.

In the $t=0.72$ s contour plot the high pressure location is along the lower surface of the bubble away from the cylinder. This is somewhat anomalous. It arises from the collision of two irregular portions of the bubble surface during the recompression process. The highest pressure location quickly returns to the base of the cylinder.

At $t=0.76$ s the pressure contours indicate a negative pressure at the tip of the fluid layer expanding outward across the base of the cylinder. The corresponding high pressure location is near the outer edge of the re-entrant jet striking the base. Apparently the radial expansion of the thin jet layer across the base of the cylinder is fast enough to produce a small region of negative pressure.

Pressure contours at $t=0.78$ and $t=0.8$ s reflect the unphysical low pressures at the location where the code loses resolution of the recompressed bubble. Just before this loss the bubble pressure has returned to about 40 psi, corresponding to a bubble volume that is 95 times larger than its initial volume.

The axial force history on the cylinder during the second part of the calculation ($t=0.7$ to 0.8 s) is shown in Fig. 9. Unfortunately, the large negative pressure at the end of the calculation when the bubble is lost causes a large negative force on the cylinder and makes it difficult to estimate the earlier values. (The computed data was accidentally erased before the postprocessor could be used to redo the plot with the negative pressures removed!) In any case one can estimate the plateau in the force at $t=0.76$ s to be approximately 5900 tons when adjusted for units and the total area of the cylinder. Just before the large negative pressure destroys the calculation, the force is about 15,700 tons.

During the total 0.8 s interval modeled, surface waves could not have traveled very far. Assuming a surface disturbance wave length equal to the diameter of the cylinder, the surface wave speed would be roughly 36 ft/s. Thus, waves could travel outward only about 29 ft, which is near the outer boundary of the computed region. The vector plots suggest that there has been some wave interaction

with the fixed surface height at this boundary. Such small surface waves, however, are not likely to have much effect on the bubble collapse or on the net axial force experienced by the cylinder.

SUMMARY AND DISCUSSION

The large volume change in the gas bubble and the rapidly changing time scales in this problem make it a difficult computation. Nevertheless, FLOW-3D does a remarkable job up until the time the recompressed bubble can no longer be resolved.

The CPU time to process the first portion of the calculation to a problem time of 0.7 s was 4.89 hours on a MicroVAX II computer (it would be a little over one hour on a SUN 4 workstation). To complete the second portion of the problem from 0.7 s to 0.8 s another 4.28 hours was required. This time was unnecessarily long and resulted from an overly conservative convergence criterion for the pressure iterations.

To confirm the influence of the convergence level and to check whether or not the void closure model used in FLOW-3D was causing unrealistic pressures (and forces), a repeat calculation was performed for the continuation of the problem from 0.7 s to 0.8 s. In this case the convergence criterion was doubled (from 0.005 to 0.01) and the void closure option was disabled (IFPK=0). The CPU time for this repeat computation was 2.26 hours, or about half the time required previously, which confirms the fact that the original convergence level was too tight.

Figure 10 shows the final results of this alternative calculation. Numerous small voids can be seen in the vector plot, but these are not recognized by the code, which treats these regions as though they are completely full of fluid. The pressure contours do indicate a negative pressure near the outer edge of the cylinder base, which is caused by the dynamics and not by the artificial void closure that was active in the earlier calculation.

A careful comparison of the two calculations during the final bubble collapse period indicated no substantial differences in the results except that the large negative pressure observed at the end of the first calculation did not occur in the repeat calculation. This, of course, was expected since the void-packing option was turned off.

We conclude that either calculation is acceptable as long as the bubble is resolved. Neither calculation can be trusted beyond a time of about $t=0.78$ s. To proceed past this time the entire calculation must be repeated with much finer grid resolution over a region encompassing the full width of the cylinder and extending several feet below the base of the cylinder.

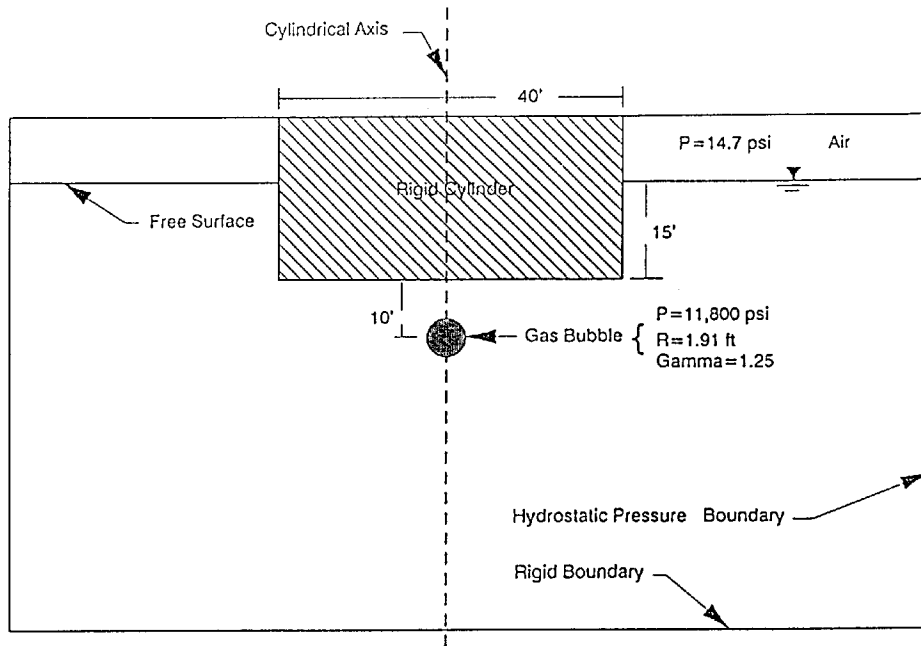


Fig. 1. Schematic of underwater explosion problem.

```

DTRC TEST CASE
$XPUT
  REMARK='UNITS: FT, S, PSI'
  ITB=1, IORDER=3, IPDIS=1,
  CYL=1.0, AVRCK=-2.1,
  GZ=-32.2, GAMMA=1.25, PVOID=14.7,
  RHOF=0.01347, REMARK='RHO REDUCED BY 144 FOR P IN PSI',
  WR=5, FLHTR=0.0, FBCTYP=1.0,
  DELT=1.0E-4, EPSI=0.005,
  TWFIN=0.7, PRDPT=100.,
  TEDIT(1)=0.1, TPLTD(1)=0.02,
  TEDIT(2)=0.55, TPLTD(2)=0.1,
  TEDIT(3)=0.7, TPLTD(3)=0.01,
SEND
$MESH
  NXCELT=27,
  PX(2)=20.0, PX(3)=50.0,
  SIZEX(1)=0.5, NXCELL(1)=15,
  NYCELT=1,
  PY(2)=23.0,
  NZCELT=55,
  PZ(1)=-75., PZ(2)=-25., PZ(3)=-15., PZ(4)=10.,
  SIZEZ(2)=0.5, NZCELL(2)=13, NZCELL(3)=12,
SEND
$SOBS
  NOBS=1,
  IOFO(1,1)=1,
  CRXY(1)=1.0, CC(1)=-20.0, ZL(1)=-15.0, RAH(1)=20.0,
SEND
$SFL
  FLHT=0.0,
  NFLS=1, FIOH(1)=0, PREG(1)=11800.,
  FCX2(1)=1.0, FCY2(1)=1.0, FCZ2(1)=1.0,
  FCZ(1)=50.0, FCC(1)=621.352,
  FZL(1)=-30.0, FZH(1)=-20.0, FRAH(1)=3.0,
SEND
$SBF
SEND
$TEMP
SEND
$GRAFC
  NVPLTS=1,
  NCPLTS=1,
  ILOC(1)=2, JLOC(1)=2, KLOC(1)=44,
  ILOC(2)=2, JLOC(2)=2, KLOC(2)=31,
  NHINF=1, IFXR(1)=17, KFZB(1)=43,
  WINTL(1)='CENTER OF BOTTOM SURFACE',
  WINTL(2)='CENTER OF INITIAL BUBBLE',
SEND
$PARTS
SEND

```

Fig. 2. Input file for FLOW-3D.

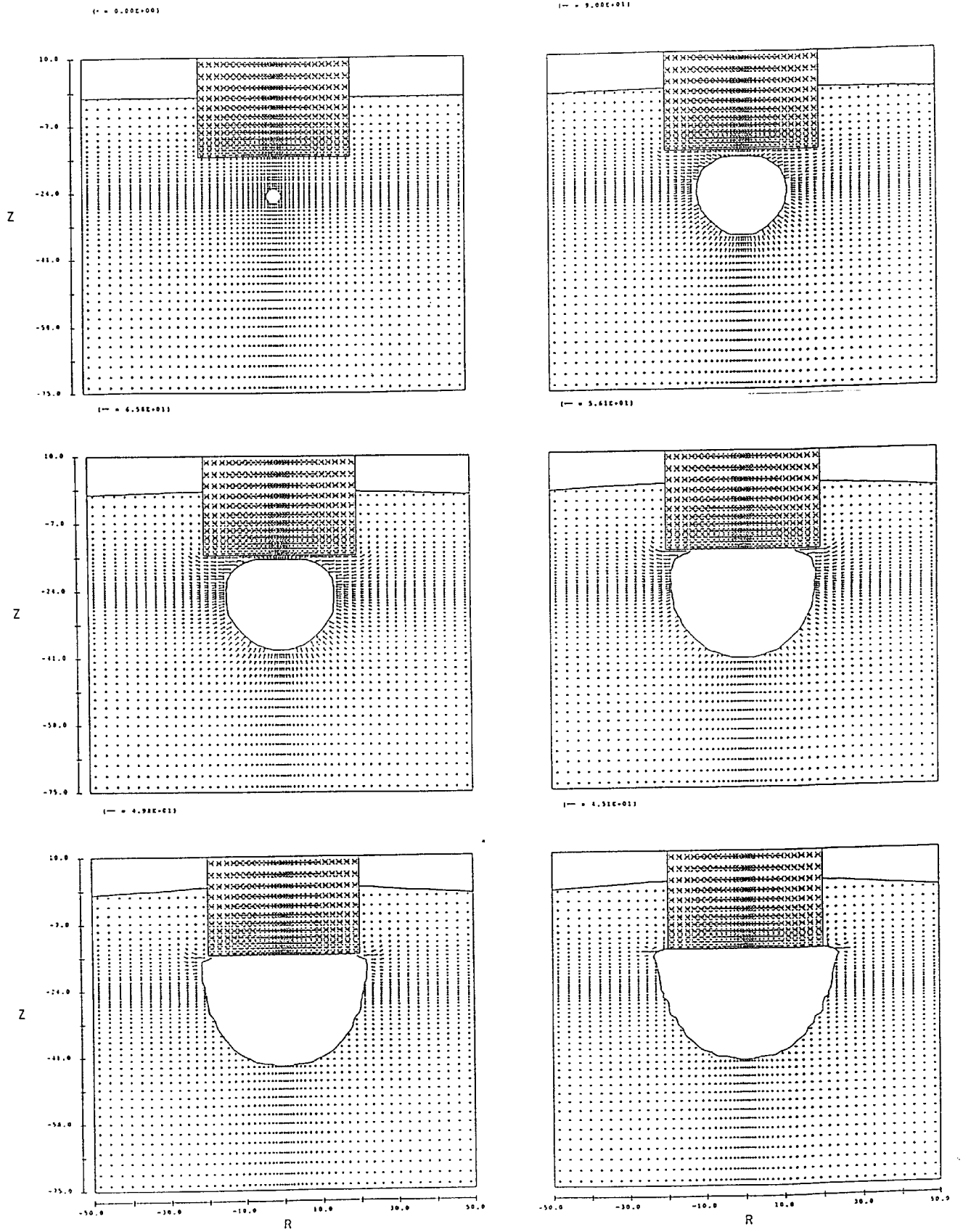


Fig. 3. Computed velocities and fluid configuration at 0.0, 0.06, 0.10, 0.20, 0.30, and 0.40 seconds.

